International Communications in Heat and Mass Transfer 139 (2022) 106420

Contents lists available at ScienceDirect

International Communications in Heat and Mass Transfer

journal homepage: www.elsevier.com/locate/ichmt

# Convective-radiative magnetized dissipative nanofluid (CNTs-water) transport in porous media, using Darcy–Brinkman–Forchheimer model

Muzamil Hussain [a,b,c,*], Mikhail Sheremet [a]

[a] Laboratory on Convective Heat and Mass Transfer, Tomsk State University, Tomsk 634050, Russia
[b] Department of Mathematics, COMSATS University Islamabad, Park Road Chak Shahzad Islamabad, 44000, Pakistan
[c] Department of Mathematics, University of the Poonch Rawalakot, Rawalakot 12350, Pakistan

ARTICLE INFO

*Keywords:*
Carbon nanotubes (CNTs)
Nanofluid flow
Inclined magnetic field
Poros media
Darcy–Brinkman–Forchheimer model
Non-similarity

ABSTRACT

The main objective of this investigation is to deliberate the novel analysis of buoyancy-driven nanofluid flow across a vertical stretching surface embedded in a porous medium with the consideration of an inclined magnetic field and heating effects caused by viscosity, thermal radiations, and heat source factor. A material made of glass ball is applied as the porous medium. Water is regarded as a base fluid, while carbon nanotubes are termed as the nanoparticles. The governing equations are formulated by employing fundamental laws. With the application of appropriate non-similar transformations, the emerging flow system is translated into dimensionless differential form. The obtained coupled, non-similar system of nonlinear partial differential equations (PDEs) is tackled by employing local non-similarity technique up to second level of iterations in conjunction with the Lobatto III technique in MATLAB. According to the findings, increasing the Hartmann number diminishes fluid velocity while augmentation in radiation parameter and nanoparticle volume fraction raises the temperature profile. Moreover, nanofluids contain MWCNTs as such nanoparticles exhibit larger estimations of Nusselt number than SWCNTs-water nanofluid. Authors introduced appropriate transformations for considered problem and argued the local non-similarity approach for simulating the dimensionless structure. To the best of authors' observations, no such study is yet published in literature.

## 1. Introduction

In today period of nanotechnology, nanofluids, engineering of converting nanoparticles into colloidal dispersions liquid medium which belonging to a new classification of heat transferring in fluids which is highly intensive work in the last few years. For the formation of nanofluids, metal oxides or carbon-based materials like graphene, CNTs, graphite, diamond, and a variety of nitrides and carbides, are potential nanomaterials Fig. 1. The attractive aspects that have make the most interesting in nanofluid is thermal property and conductive nature which indicates the ability of a "nanofluid" for the conduction of heat. The applications of "nanofluid" with lower viscosity and higher conductivity are very promising between nanomaterial and fluid-based nanomaterial. Research on nanofluid can be enriched and extended through exploring new aspects of this smart fluid. Some of studies that presented the applications associated with the nanofluids may be found in Ref. [1–9]. Bhatti et al. [10] examined the thermal features of Williamson unsteady nanofluid flow that is confined by two parallel circular plates across a porous media. Shahid et al. [11] assessed the MHD bioconvective Carreau nanofluid flow over a paraboloid porous surface with the considerations of chemical reaction and activation energy. Alazwari et al. [12] examined the heat transfer and entropy generation of the first-grade viscoelastic mono nanofluids past a stretching sheet. Abu-Hamdeh et al. [13] investigated computationally a boundary-layer flow of engine-oil-based nanofluids past a porous stretching plate as an element of parabolic trough solar collector under an influence of thermal radiation, and Cattaneo-Christov heat flux. It has been found that a raise of the Reynolds number, Brinkmann number and Eckert number characterizes the entropy production enhancement. Aouinet et al. [14] scrutinized numerically the turbulent boundary layer flow of three different nanofluids past a flat plate. Authors revealed that a growth of the nanoparticle's concentration has a minor influence of the shear stress at the wall. Jamshed et al. [15] analyzed the unsteady flow, heat transfer and entropy generation of a Casson nanosuspension over an extending surface. It has been ascertained that positive variation in volume fraction and Casson parameters reduces the velocity profiles.

* Corresponding author at: Laboratory on Convective Heat and Mass Transfer, Tomsk State University, Tomsk 634050, Russia.
*E-mail address:* muzamil@upr.edu.pk (M. Hussain).

https://doi.org/10.1016/j.icheatmasstransfer.2022.106420

Available online 11 October 2022

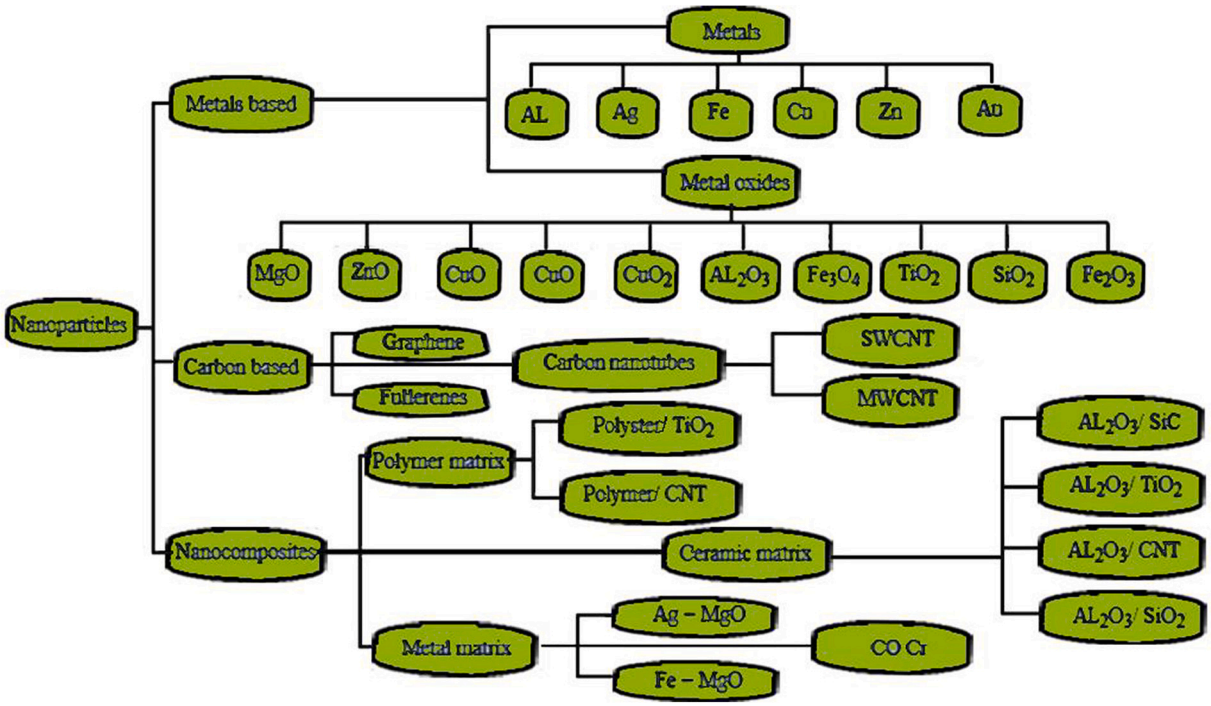


**Fig. 1.** Illustration of metal-based, carbon-based, and nanocomposites nanoparticles.

Maleki et al. [16] calculated fluid flow and heat transfer regarding pseudo-plastic nanofluid across a moving permeable flat surface with the impacts of heat absorption/generation and viscous dissipation. Authors showed that the energy transport degradation can be found for growing of injection parameter, nanoadditives concentration and heat generation parameters, while the heat transfer enhancement is for high values of heat absorption parameter, velocity ratio and suction parameter. Other interesting outcomes on nanofluids flow and heat transfer can be found in [17–20].

Carbon nanotubes (CNTs) are preferable to typical nanomaterials in almost any activity requiring electrical conductivity, high strength, durability, lightweight, and thermal conductivity. CNTs have been extensively researched in recent years due to their exceptional thermal features. In general, CNTs-nanofluids research has evolved in many different areas, attracting a significant deal of attention from researchers. For example, CNTs-nanofluids can, increase boiling heat transfer and reduce the Leidenfrost effect in a quenching process, improve bubble absorption in a thermally driven absorption system and improve the heat-transfer utility of a heat pipe in a solar collector. CNTs exhibit ultra-high thermal conductivity (2000–6000), which is significantly higher than that of metallic or oxide nanomaterials used in nanofluids. Furthermore, CNTs with a high aspect ratio offer outstanding heat transmission properties. CNTs have good heat transmission performance along the length direction. Jalili et al. [21] experimentally studied the performance regarding heat transfer for refrigeration cycle with CNTs nanoparticles in the working fluid and show that the different concentrations of nanoparticles have different impacts on the refrigerator performance. Gul et al. [22] examined the rate of heat and mass transport of nanofluid in conical space of cone and disc while accounting for MHD and CNT's. Berrehal and Makinde [23] used the homotopy perturbation approach to examine the heat transfer properties of a CNTs-water nanofluid flow between two nonparallel surfaces. Xia et al. [24] assessed the nonlinear mixed convective micropolar nanofluid (CNTs+$C_2H_2F_4$) flow in the presence of numerous slip conditions, joule heating and activation energy across a slandering surface. Hussain et al. [25] reported the electromagnetic radiative water-based CNTs nanofluid flow with entropy generation over a convectively heated surface. Hossain et al. [26] investigated the unsteady, mixed convective, MHD kerosene-based CNT nanofluid in a squared cavity with the impacts of radiative heat flux.

Fluid flow and heat transmission in porous media have piqued a considerable attention of researchers in recent decades. This is primarily due to the several applications of fluid flow through porous medium, including transpiration cooling, radioactive nuclear waste storage, separation processes in chemical sectors, filtration, groundwater pollution, aquifers transport processes, fibre insulation, and geothermal extraction. Recently, the technique of employing both porous media and nanofluid has attracted a lot of interest, leading to a lot of research in this field. Mahdi et al. [27] reviewed the impacts of several parameters on thermophysical properties of nanofluids across different porous media geometries and deduce that convection heat transfer is increased with porous media. Kasaeian et al. [28] examined the simultaneous use of porous media and nanofluids for heat transfer augmentation in thermal systems with varying flow regimes, and boundary conditions. Albojamal and Vafai [29] used the discrete particle model (DPM) to explore the particle entrapment and heat transfer properties of nanoparticles for nanofluid transport over porous media. Mandal et al. [30] inspected the impacts of surface undulation on MHD mixed nanobioconvective heat transfer in a porous enclosure. Shahzad et al. [31] examined the magnetohydrodynamics (MHD) nanofluid flow past a permeable stretched surface with the assumptions of heat generation, porous media, viscous dissipation, and Ohmic heating. Anusha et al. [32] investigated MHD couple stress laminar water-based hybrid nanofluid flow across a shrinking / stretching surface with the concepts of inclined magnetic field and porous media.

Magnetic field is employed in many areas of modern technology, most notably electromechanics, industrial equipment, and engineering applications. The study of the magnetic characteristics and behavior of electrically conducting fluids is known as magnetohydrodynamics (MHD). Magnetohydrodynamics has several important applications, including biomechanics, blood flow measurements, plasma studies, MHD generators, petroleum technologies, etc. The intensity of the magnetic field influences the behavior of nanofluid flow. It is understood that nanofluids with MHD effects have the capacity to modify flow and

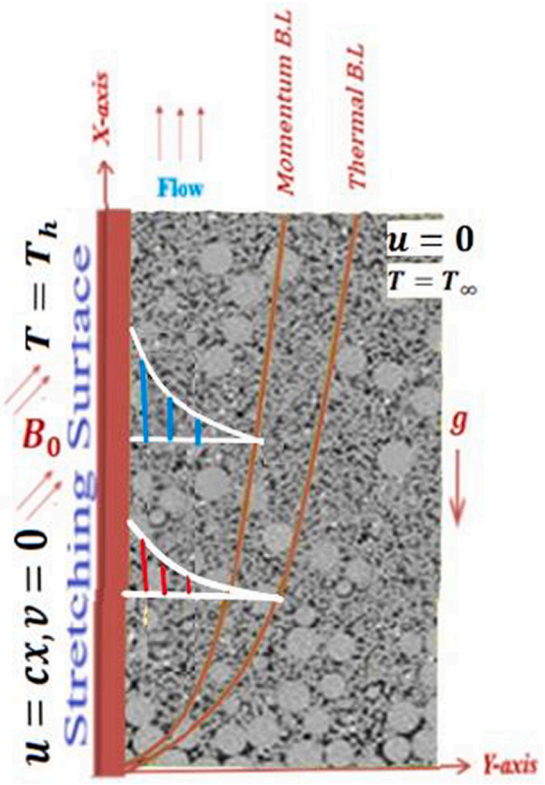


**Fig. 2.** Flow illustration for current model.

improve heat transfer from electrically conductive fluids. Refs. [33–38] summarize a few noteworthy recent findings that support the notion of MHD and porous medium of nanofluid. Padmaja and Kumar [39] examined the nanofluid flow over a vertical surface embedded in a porous medium with the considerations of Ohmic heating and buoyancy effects. Authors present a comprehensive study regarding heat and mass transfer of MHD nanofluid, along with first-order chemical reaction and radiative heat flux. Haq et al. [40] performed an analytical simulation for thermos-migration nanofluid flow subject to the magnetic field, porous media and thermal radiation across a moving wedge.

Enthused by the above-mentioned literature, the current study is focused on non-similar analysis of MHD incompressible flow of nanofluid across a permeable stretching sheet with the effects of viscous dissipation, thermal radiation, and heat source factor. The influence of porosity and gravity parameters are also considered. Water is considered as the base fluid, because of weak thermal conductivity, it could be altered by the addition of nanoparticles [41–43]. More specifically, water is commonly utilized in industry and water is a valuable component for the survival of nature since it is generally available, moderately inexpensive, and capable of dissolving to form a solution, suspension, or colloidal suspension. As a result, numerous scientists and researchers are clamoring for more information about water and its associated properties. Owing to its excellent features like good conductivity, durability, and lightweight, SWCNTs and MWCNTs are referred to as nanoparticles in this study. As a porous medium, the substance consisting of glass balls is used. Darcy-Forchheimer-Brinkman model is imposed here to express the features of porous medium. To simulate the momentum and energy equations, single-phase (Tiwari-Das) model is adopted. The fundamental model of partial differential equations (PDEs) is reframed into the structure of dimensionless equations implementing the non-similar transformation, which are tackled through the local non-similarity approach with the consideration of bvp4c package in MATLAB. Tables and graphs are used to compute and discuss the generated findings. The concluding remarks and comparative analysis are also included.

**Table 1**
Thermo-physical values of MWCNTs, SWCNTs and water.

| Materials | $\beta\times10^{-5}$ (1/K) | $c_p$(J/kgK) | $\rho$ (kg/m$^3$) | k(W/mK) | $\sigma(\Omega m)^{-1}$ | $Pr$ |
|---|---|---|---|---|---|---|
| MWCNTs | 44 | 796 | 1600 | 3000 | $1.9\times10^4$ | – |
| SWCNTs | 27 | 425 | 2600 | 6600 | $10^6$–$10^7$ | – |
| Pure Water | 21 | 4179 | 997.1 | 0.613 | 0.05 | 6.2 |
| Glass Balls | – | – | – | 1.05 | – | – |

**Table 2**
Entrenched dimensionless parameters.

| Symbols | Name / Expression | Default values |
|---|---|---|
| $\varepsilon$ | Porosity | 0.9 |
| $\alpha$ | Inclined angle of magnetic field | 60$^o$ |
| $F_c$ | Forchheimer coefficient $= \frac{1.75}{\sqrt{150\varepsilon^3}}$ | 0.167 |
| $\gamma$ | Darcy porosity parameter $= \frac{\upsilon}{cK}$ | 0.7 |
| $Da$ | Darcy number $= \frac{\sqrt{K}}{l}$ | 0.02 |
| $Ha$ | Hartmann number $= \frac{\sigma_f {B_0}^2}{\rho_f c}$ | 0.5 |
| $Ri$ | Richardson number $= \frac{g\beta(T_h - T_\infty)}{c^2 l}$ | 0.5 |
| $Pr$ | Prandtl number $= \frac{\mu c_p}{k}$ | 6.2 |
| $Nr$ | Radiation parameter $= \frac{16\sigma^* T_\infty^3}{3k^* k_f}$ | 0.5 |
| $Q^*$ | Heat source / sink parameter $= \frac{Q_0}{c(\rho c_p)_f}$ | 0.1 |
| $Ec$ | Eckert number $= \frac{(cl)^2}{c_p(T_h - T_\infty)}$ | 0.05 |
| $\phi$ | Nanoparticles concentration | 0.02 |

## 2. Mathematical formulation

Consider steady, two-dimensional, incompressible, laminar, nanofluid flow across a vertical stretching surface embedded in a porous medium, where the stretching surface is placed along the $Y$-direction. Fig. 2 demonstrates the flow model with coordinate system. As the porous medium, a material composed of glass balls is used because the porous glass-material has many advantages such as good thermal stability, high strength, greater pores volume and large specific surface areas that are commonly elected for various applications such as lightweight concrete, biomaterials, insulations, and filter systems. To express the attributes of porous media, the Darcy-Forchheimer-Brinkman model is assumed. The single-phase model simulates the momentum and energy equations. SWCNTs and MWCNTs are considered nanoparticles in a water-based nanofluid. The flow is subjected to a uniform inclined magnetic field having strength $B_0$. While designing energy expression, the effects of heat sources and thermal radiation are also considered. Convective heat transfer is factored into the equation. The flow is induced by the sheet stretching in its own plane with the surface velocity $U_w(x) = cx$ where $c$ having dimension (time)$^{-1}$ is a positive constant. The stretching surface temperature $T_h$ is considered to be higher than the ambient temperature $T_\infty$. The base fluid (water) and the nanoparticles are also expected to be in thermal equilibrium. Table 1 lists the thermophysical values of nanoparticles, base fluid and porous materials. The governing system for current flow in the presence of thermal radiation, heat source factor, inclined magnetic field and subjected to the Boussinesq approximation can be stated as:

$$\frac{\partial u}{\partial x} + \frac{\partial v}{\partial y} = 0, \tag{1}$$

$$\frac{1}{\varepsilon^2}\left[u\frac{\partial u}{\partial x}+v\frac{\partial u}{\partial y}\right]=\frac{\upsilon_{nf}}{\varepsilon}\frac{\partial^2 u}{\partial y^2}-\upsilon_{nf}\frac{u}{K}-\frac{F_c}{\sqrt{K}}u^2-\frac{\sigma_{nf}}{\rho_{nf}}B_0^2 u.sin^2\alpha+g\frac{(\rho\beta)_{nf}}{\rho_{nf}}(T-T_\infty), \tag{2}$$

$$u\frac{\partial T}{\partial x}+v\frac{\partial T}{\partial y}=\frac{k_{eff}}{(\rho c_p)_{nf}}\frac{\partial^2 T}{\partial y^2}-\frac{1}{(\rho c_p)_{nf}}\frac{\partial q_y}{\partial y}+\frac{Q_0}{(\rho c_p)_{nf}}(T-T_\infty)+\frac{\varepsilon\mu_{nf}}{(\rho c_p)_{nf}}\left(\frac{\partial u}{\partial y}\right)^2+\frac{\varepsilon\mu_{nf}}{(\rho c_p)_{nf}}\frac{1}{K}u^2, \tag{3}$$

(See Table 2).

The radiative heat flux $q_y$ is defined as follows (using the Rosseland approximation) [44]:

$$q_y=-\frac{4\sigma^*}{3k^*}\frac{\partial T^4}{\partial y} \tag{4}$$

Here ($k^*(m^{-1})$) is Rosseland absorption coefficient and ($\sigma^*=5.67\times10^{-9}(W/m^2K^4)$) signifies the Stephan–Boltzmann constant. Considered that the temperature variations within the flow are such that $T^4$ can be characterized as a linear function of temperature, implying that it exhibits Taylor series expansion. After simplification, we get:

$$u\frac{\partial T}{\partial x}+v\frac{\partial T}{\partial y}=\frac{k_{eff}}{(\rho c_p)_{nf}}\frac{\partial^2 T}{\partial y^2}+\frac{16\sigma^* T_\infty^3}{3k^*(\rho c_p)_{nf}}\frac{\partial^2 T}{\partial y^2}+\frac{Q_0}{(\rho c_p)_{nf}}(T-T_\infty)+\frac{\varepsilon\mu_{nf}}{(\rho c_p)_{nf}}\left(\frac{\partial u}{\partial y}\right)^2+\frac{\varepsilon\mu_{nf}}{(\rho c_p)_{nf}}\frac{1}{K}u^2. \tag{5}$$

Here, $u$ and $v$ characterize the velocity components, while $T$ is the temperature, $\varepsilon$ is the porosity, $g$ is the gravitational acceleration, and $k_{eff}$ $=(1-\varepsilon)k_{pm}+\varepsilon k_{nf}$ where $k_{pm}$ is the thermal conductivity of solid material of porous medium. $F_c=\frac{1.75}{\sqrt{150\varepsilon^3}}$ is the Forchheimer coefficient. $K=\frac{\varepsilon^3 ds^2}{150(1-\varepsilon)^2}$ represents the permeability while $ds$ describes the average particle size of the porous bed. Also, in the above-mentioned governing system various mathematical notations regarding nanofluid are used, where $(\rho\beta)_{nf}$ is the volumetric thermal expansion coefficient, $\sigma_{nf}$ is the electrical conductivity of nanofluid, $\rho_{nf}$ is the nanofluid density, $(\rho c_p)_{nf}$ signifies the specific heat of nanofluid, $\mu_{nf}$ indicates the viscosity of the nanofluid and $k_{nf}$ specifies the thermal conductivity of nanofluid. These effective physical properties can be defined [45–49]:

Volumetric thermal expansion coefficient:

$$(\rho\beta)_{nf}=(1-\phi)(\rho\beta)_{bf}+\phi(\rho\beta)_{np} \tag{6}$$

Electrical conductivity:

$$\sigma_{nf}=\left\{1+\frac{3\left(\frac{\sigma_{np}}{\sigma_{bf}}-1\right)\phi}{\left(\frac{\sigma_{np}}{\sigma_{bf}}+2\right)-\left(\frac{\sigma_{np}}{\sigma_{bf}}-1\right)\phi}\right\}\sigma_{bf} \tag{7}$$

Density:

$$\rho_{nf}=(1-\phi)\rho_{bf}+\phi\rho_{np} \tag{8}$$

Volumetric specific heat:

$$(\rho C_p)_{nf}=(1-\phi)(\rho C_p)_{bf}+\phi(\rho C_p)_{np} \tag{9}$$

Viscosity:

$$\mu_{nf}=\frac{\mu_{bf}}{(1-\phi)^{2.5}} \tag{10}$$

Thermal conductivity:

$$\frac{k_{nf}}{k_{bf}}=\frac{1-\phi+2\phi\left(k_{np}/(k_{np}-k_{bf})\right)ln\left((k_{np}+k_{bf})/2k_{bf}\right)}{1-\phi+2\phi\left(k_{bf}/(k_{np}-k_{bf})\right)ln\left((k_{np}+k_{bf})/2k_{bf}\right)} \tag{11}$$

Associated boundary conditions:

$$u=U_w(x)=cx, v=0, T=T_h \text{ at } y=0,$$

$$u=0, v=0, T=T_\infty \text{ as } y\to\infty \tag{12}$$

Introducing the transformations as:

$$\eta=\sqrt{\frac{U_w}{\upsilon x}}y, \xi=\frac{x}{l}, \theta(\xi,\eta)=\frac{T-T_\infty}{T_h-T_\infty}, u=U_w\frac{\partial f}{\partial\eta}, v=-\sqrt{c\upsilon}\left(f+\xi\frac{\partial f}{\partial\xi}\right). \tag{13}$$

Eq. (1) is trivially satisfied while the rest of system takes the following form:

$$\frac{\partial^3 f}{\partial\eta^3}=\frac{A2}{\varepsilon A1}\left[\left(\frac{\partial f}{\partial\eta}\right)^2-f\frac{\partial^2 f}{\partial\eta^2}+\xi\left(\frac{\partial f}{\partial\eta}\frac{\partial^2 f}{\partial\xi\partial\eta}-\frac{\partial^2 f}{\partial\eta^2}\frac{\partial f}{\partial\xi}\right)\right]+\epsilon\gamma\frac{\partial f}{\partial\eta}+\frac{\varepsilon}{A1}\left[A2\frac{F_c}{Da}\xi\left(\frac{\partial f}{\partial\eta}\right)^2+A3Ha\frac{\partial f}{\partial\eta}sin^2\alpha-A4Ri\xi^{-1}\theta\right], \tag{14}$$

$$\left(\frac{A5+Nr}{A6Pr}\right)\frac{\partial^2\theta}{\partial\eta^2}=\xi\left(\frac{\partial f}{\partial\eta}\frac{\partial\theta}{\partial\xi}-\frac{\partial\theta}{\partial\eta}\frac{\partial f}{\partial\xi}\right)-f\left(\frac{\partial\theta}{\partial\eta}\right)-\frac{\epsilon\xi^2 EcA1}{A6}\left(\gamma\left(\frac{\partial f}{\partial\eta}\right)^2+\left(\frac{\partial^2 f}{\partial\eta^2}\right)^2\right)-\frac{Q^*}{A6}\theta, \tag{15}$$

Associated dimensionless boundary conditions are:

$$\frac{\partial f}{\partial\eta}(\xi,0)=1, f(\xi,0)+\xi\frac{\partial f}{\partial\xi}(\xi,0)=0, \theta(\xi,0)=1,$$

$$\frac{\partial f}{\partial\eta}(\xi,\infty)=0, \theta(\xi,\infty)=0 \tag{16}$$

Also, expressions $A1$, $A2$, $A3$, $A4$, $A5$, $A6$ and $A7$ are defined as:

$$A1=\frac{\mu_{nf}}{\mu_{bf}}, A2=\frac{\rho_{nf}}{\rho_{bf}}, A3=\frac{\sigma_{nf}}{\sigma_{bf}}, A4=\frac{(\rho\beta)_{nf}}{(\rho\beta)_{bf}}, A5=\frac{k_{eff}}{k_{bf}}, A6=\frac{(\rho c_p)_{nf}}{(\rho c_p)_{bf}}, A7=\frac{k_{nf}}{k_{bf}}.$$

The parameters of the physical quantities of interests like skin friction, and Nusselt number, are specified as:

$$C_f=\frac{\tau_w}{\rho_f U_w{}^2}, \text{and } N_u=\frac{x.q_w}{k_f(T_h-T_\infty)}. \tag{17}$$

Here $\tau_w$ signifies the shear stress, and $q_w$ is the heat flux defined as:

$$\tau_w=\mu_{nf}\left(\frac{\partial u}{\partial y}\right)_{y=0}, \text{and } q_w=-\left[k_{eff}+\frac{16\sigma^* T_\infty^3}{3k^*}\right]\left(\frac{\partial T}{\partial y}\right)_{y=0} \tag{18}$$

After using the above-mentioned transformations with Eq. (18), Eq. (17) can be stated in the following dimensionless form as:

$$Re^{\frac{1}{2}}C_f=A1\xi^{-1}\left(\frac{\partial^2 f}{\partial\eta^2}\right)_{\eta=0}, \text{and } Re^{-\frac{1}{2}}N_u=-\xi[A5+Nr]\left(\frac{\partial\theta}{\partial\eta}\right)_{\eta=0}. \tag{19}$$

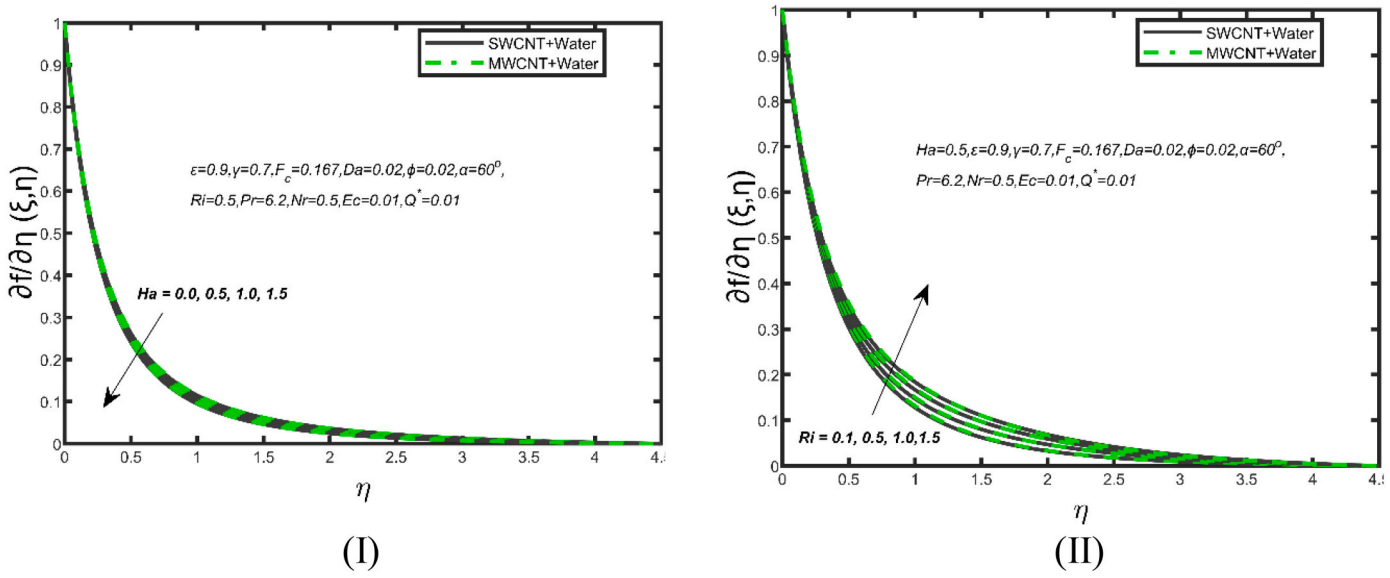


**Fig. 3.** Velocity profiles for deviating estimations of (I) *Ha* and (II) *Ri*.

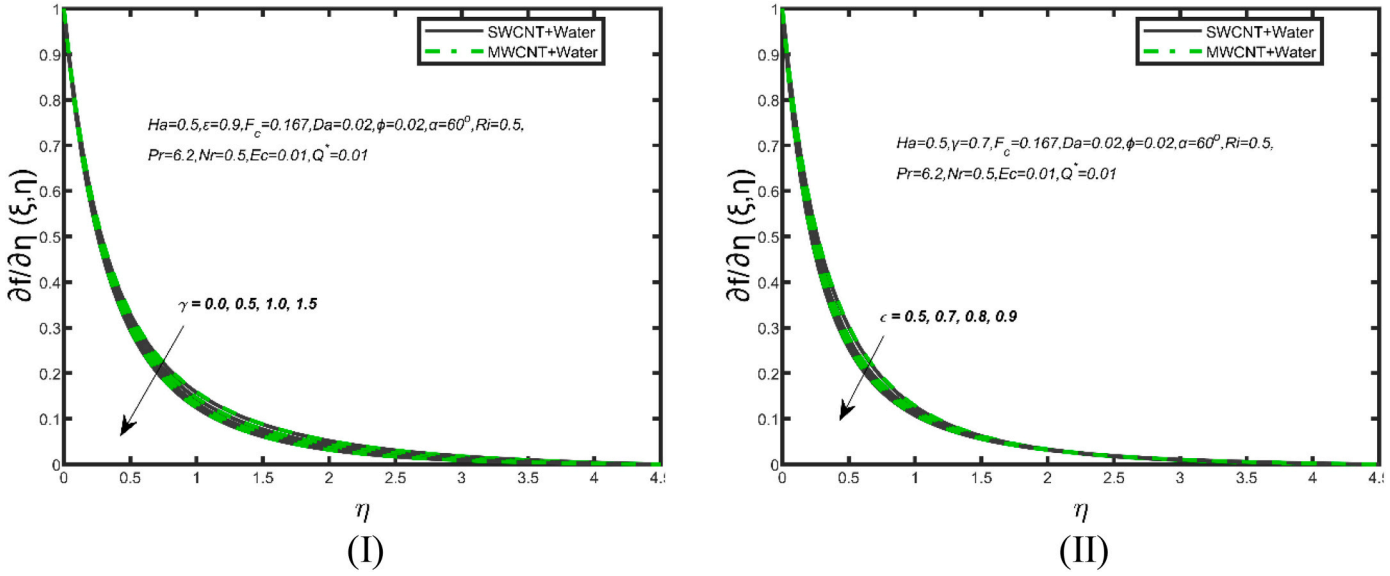


**Fig. 4.** Velocity profiles for deviating estimations of (I) $\gamma$ and (II) $\varepsilon$.

## 3. Numerical procedure

While studying boundary layer, similarity and non-similarity techniques are two distinct approaches to solving the fluid flow problems. The solution process via similarity approach is very simple. However, this similarity approach is not effective for various physical situations. Like, the natural or mixed convection flow across a vertical surface is in general non-similar. So, when a similarity approach fails, one has to tackle such problems employing a non-similarity technique. Many researchers [50–53] have used the non-similarity approach to solve complex fluid flow problems. Although there are numerous semi-analytical and numerical approaches for solving nonlinear coupled partial differential equations system. Here, we implement Sparrow and Yu's [54] approach of local non-similarity to tackle the transform system. Because it is most suitable for the considered problem. In this approach, to acquire a local similarity solution, terms containing $\xi$-derivatives are ignored first; later, to obtain a local non-similarity (LNS) solution, the $\xi$-derivatives are considered as another dependent function. Hence, we employed the LNS approach up to the second-truncation level with numerical algorithm bvp4c to achieve efficient results of given problem. bvp4c is a MATLAB package that employs Labatto III code. In procedure of bvp4c, the residual error module approximates numerical simulation error. All the tabular and graphical simulations of this investigation are compiled under the bvp4c tolerance criteria.

## 4. Results and discussion

The subsequent description is established on the numerical findings obtained by the scheme detailed described in the preceding section. Response of non-dimensional velocity and temperature profiles of nanofluids against the emerging physical parameters is deliberated with the help of graphical illustrations. For parametric variations of the porosity ($\varepsilon$), inclined angle of magnetic field ($\alpha$), Darcy porosity parameter ($\gamma$), Darcy number (*Da*), Richardson number (*Ri*), Radiation parameter (*Nr*), Hartmann number (*Ha*), Heat source/sink parameter

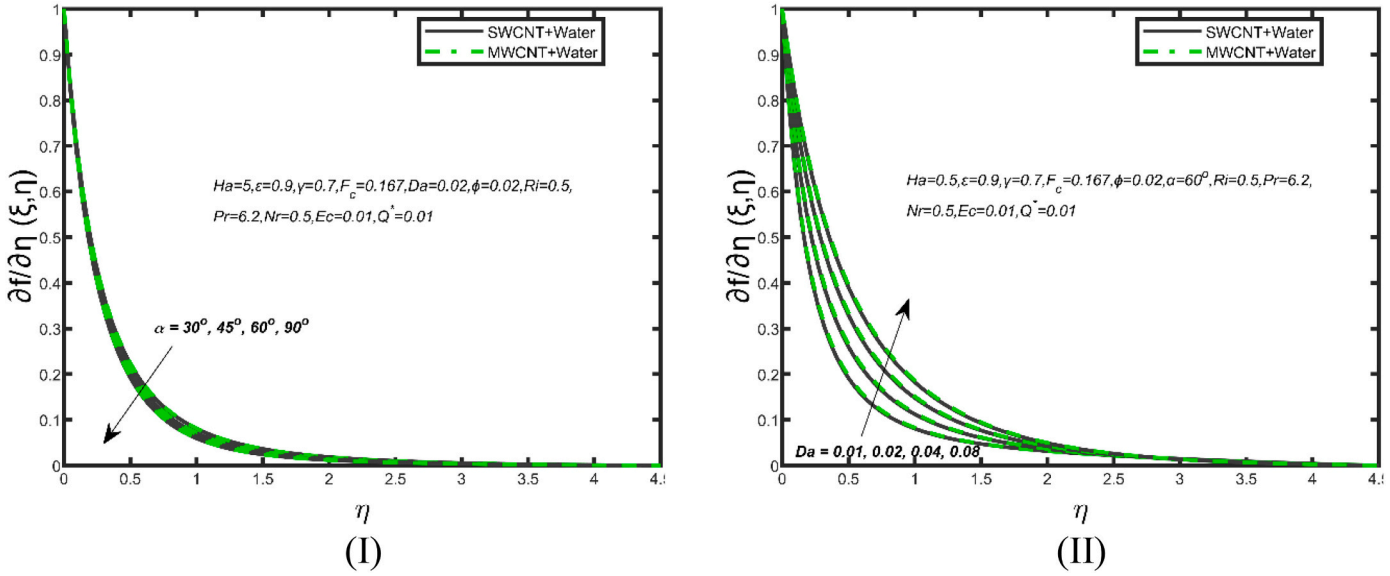


**Fig. 5.** Velocity profiles for deviating estimations of (I) $\alpha$ and (II) *Da*.

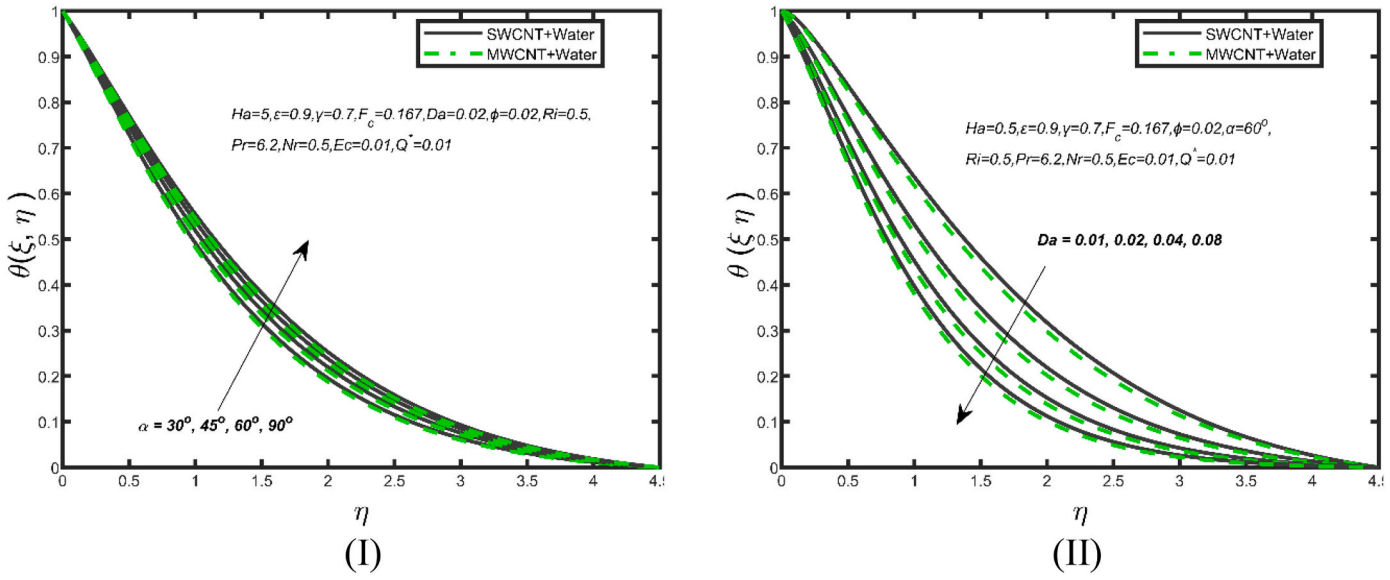


**Fig. 6.** Temperature profiles for deviating estimations of (I) $\alpha$ and (II) *Da*.

($Q^*$), Eckert number (*Ec*), nanoparticles concentration ($\phi$), and Prandtl number (*Pr*), the numerical findings for friction factor and surface heat transfer rate have been reported. The computations are carried out for water-based (*SWCNTs* and *MWCNTs*) nanofluids. Fig. 3 illustrates the response of nanofluid velocity distributions across the boundary layer against various values of Hartmann number (*Ha*) and Richardson number (*Ri*) for water-based nanoparticles of SWCNTs and MWCNTs. The influence of *Ha* on velocity profiles is shown in Fig. 3 (I). With rising *Ha* values, the velocity profiles (for both types of CNTs) drop. The Lorentz force, which opposes motion and it is responsible for decreasing fluid velocity, arises physically as a result of the applied magnetic field. The fluctuation of the velocity profile versus the Richardson number (*Ri*) is seen in Fig. 3 (II). The *Ri* represents the relationship between the buoyancy and the flow gradient terms in general. We can observe from this graph that enhancement in *Ri* increases the magnitude of the fluid flow. We may state that natural convection is negligible when $Ri < 0.1$, while forced convection is negligible when $Ri > 10$, and neither is disregarded when $0.1 < Ri < 10$. Natural convection is stronger than forced convection when the fluid has an extremely low forced velocity; otherwise, force convection is greater.

Fig. 4 (I) depicts a clear decline of the velocity distribution with a surge in the values of $\gamma$. Physically, this must be responsible for the increased fluid viscosity as a result of the increased $\gamma$. This eventually leads to a decline in momentum layer thickness. Fig. 4 (II) displays the impacts of the porosity parameter ($\varepsilon$) on the dimensionless velocity distribution. The velocity profile has been seen to decline when $\varepsilon$ increases. The consequences of the magnetic field inclination angle ($\alpha$) on the velocity profile is seen in Fig. 5 (I). It is clear that increasing $\alpha$ reduces the velocity profile of the nanofluids. The reason for this phenomenon is a rise in the angle of inclination, which causes the magnetic field to intensify. It creates the opposing force field (Lorentz force) to the flow. This force diminishes the momentum boundary layer thickness. Fig. 5 (II) presents the impacts of Darcy parameter (*Da*) on velocity profile. An increment in *Da* leads to higher velocity field. For larger *Da*, the permeability increases which produces an enhancement in fluid velocity.

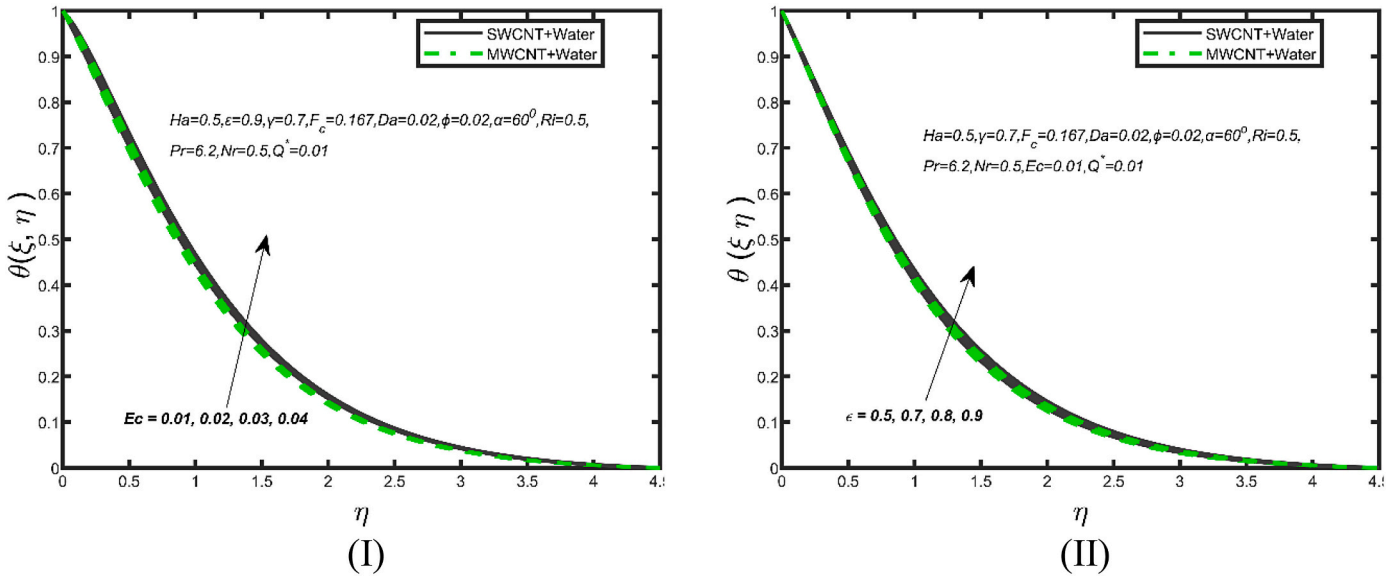


**Fig. 7.** Temperature profiles for deviating estimations of (I) *Ec* and (II) $\varepsilon$.

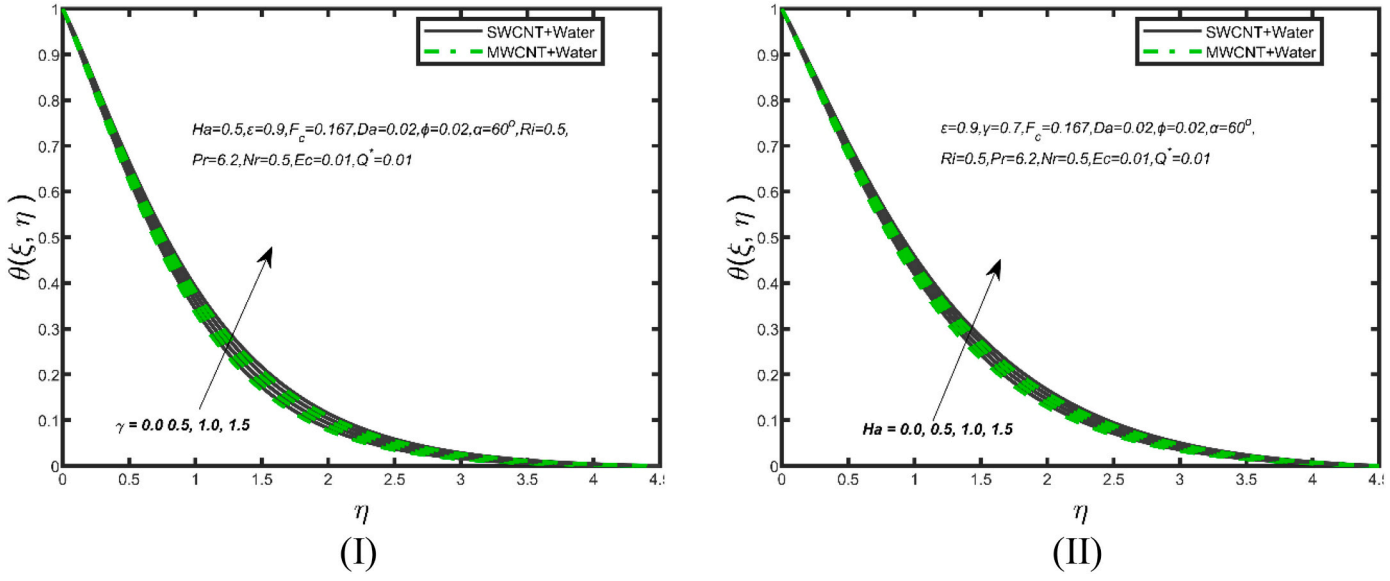


**Fig. 8.** Temperature profiles for deviating estimations of (I) $\gamma$ and (II) *Ha*.

Fig. 6 (I) exhibits the consequence of the magnetic field inclination angle ($\alpha$) on the temperature profile. It is clear that the increase in $\alpha$ surges the temperature profile of the nanofluids. The increase in angle of inclination causes the viscosity of nanofluid to strengthen due to Lorentz force, which is the cause for this outcome. Fig. 6 (II) shows the impacts of Darcy parameter on temperature profile. An increment in *Da* leads to decline in temperature field. Fig. 7 (I) depicts temperature fluctuation using the Eckert number (*Ec*). The temperature distribution of nanofluid clearly rises with an increasing *Ec*. Because a higher *Ec* indicates more dissipation, more internal energy is produced, and temperature rises consequently. Fig. 7 (II) portrays the impact of the porosity parameter ($\varepsilon$) on the temperature profile. The temperature profile for both studied water-based-SWCNTs and MWCNTs nanofluids grows significantly with increasing $\varepsilon$ across the domain.

Fig. 8 (I) exhibits the temperature field fluctuation when the Darcy porosity parameter ($\gamma$) is varied. Higher $\gamma$ values result in a stronger temperature field and a thicker thermal layer. More resistance is noticed in the presence of a porous material and this one is a responsible for higher temperature profile. Fig. 8 (II) reveals that rising *Ha* magnifies the temperature distribution. A resistive type of force will be created in the nanofluid flow due to the presence of a magnetic field. This force has the capacity to slow down the nanofluid's movement. As a result of the same force, the nanofluid obtains some heat energy. Fig. 9 (I) illustrates that the concentration of nanoparticles ($\phi$) raises the fluid temperature. Physically, raising $\phi$ improves the thermal conductivity phenomenon, which raises the thermal profile. Fig. 9 (II) depicts the effect of increasing heat generation/absorption parameter ($Q^*$) on the temperature profile. The display demonstrates that as $Q^*$ increases, so does the temperature.

Temperature variation against radiation parameter (*Nr*) is sketched in Fig. 10 (I). Increasing the estimations of *Nr* enhances the temperature profile and associated boundary layer. Thermal radiation clearly causes an increase in surface heat flow. As a result, the temperature profile of nanofluid within the boundary layer rises. Fig. 10 (II) depicts the physical relevance of the Richardson number (*Ri*) on the temperature field. The *Ri* is a nondimensional number that represents ratio of

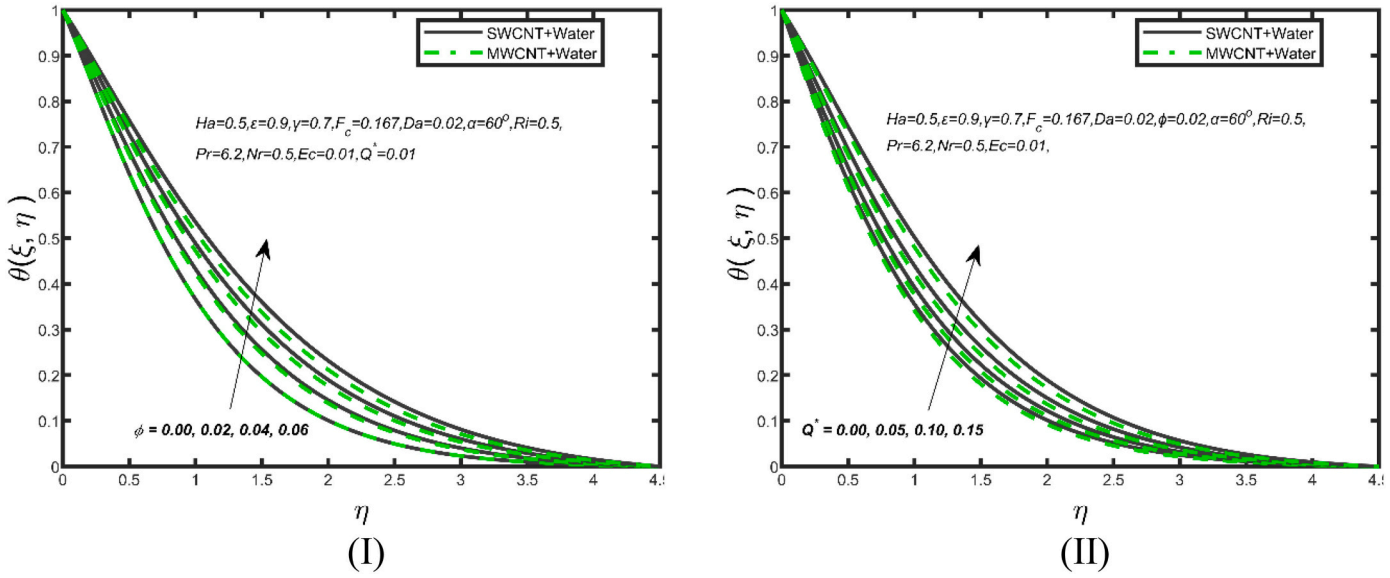


**Fig. 9.** Temperature profiles for deviating estimations of (I) $\phi$ and (II) $Q^*$.

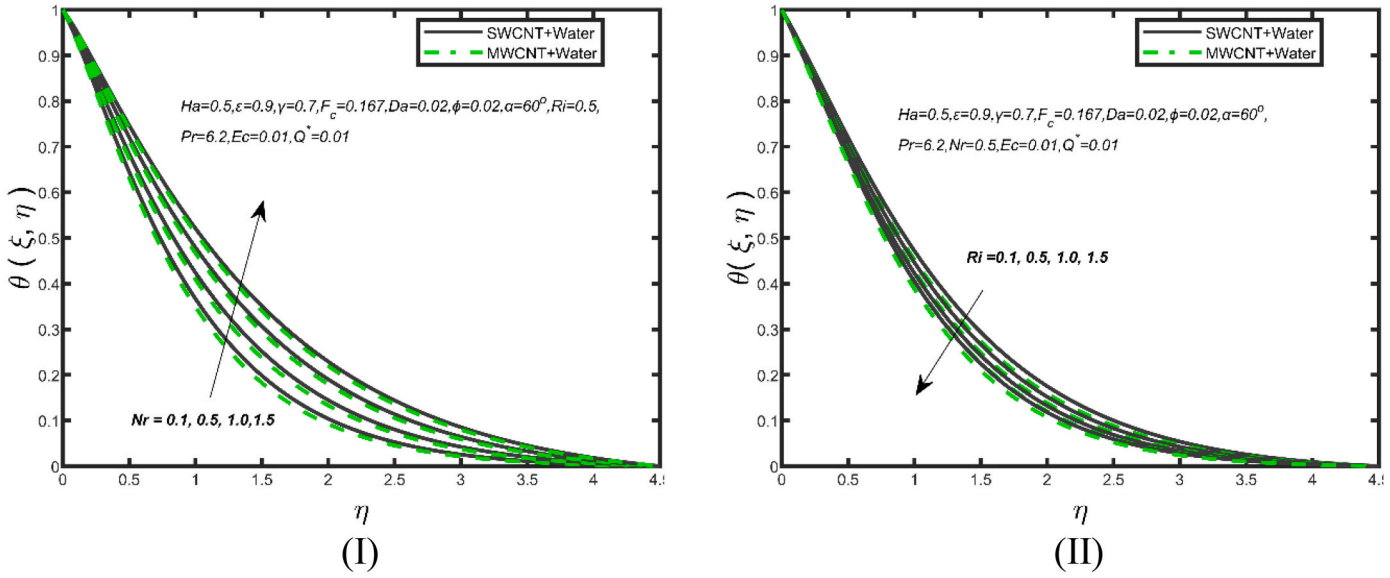


**Fig. 10.** Temperature profiles for deviating estimations of (I) *Nr* and (II) *Ri*.

buoyancy expression to flow shear term. Increasing the *Ri* increases the buoyancy factor, resulting in a decrease in the temperature profile. Computed estimations of surface drag coefficients for SWCNTs-water and MWCNTs-water nanofluids are shown in Table 3. Magnification in *Da* and *Ri* causes a decline in the coefficient of surface drag but it raises for the positive variation in $\phi$, $\varepsilon$, $\gamma$, *Ha* and $\alpha$. Table 4 contains numerical results that evaluate the variance in $Re^{-\frac{1}{2}}Nu$ against the different numerical values of emerging parameters. For *Ri* and *Nr* diminishing numerical data is obtained, whereas rising observations are anticipated for $\phi$, $\varepsilon$, $\gamma$, *Ec* and $Q^*$ at stretching surface for both considered models. Furthermore, as compared to SWCNTs-water nanofluid, MWCNTs-water nanofluid exhibits a better rate of heat transfer. Table 5 compares the current study to the previously published literature by Andersson et al. [55] and Shaiq et al. [56]. For the purposes of comparison, the common parameters were set at $\gamma = F_c = \xi = Da = \phi = Ri = Pr = Nr = Ec = Q^* = 0$, $\varepsilon = 1$ and $\alpha = 90^0$. Table 5 shows that the $-f''(0)$ results are in close accord with the previous published literature [55,56]. It reveals that the numerical solutions offered (MATLAB built-in bvp4c package) are valid in comparison to the existing literature. Table 6 also shows a comparison examination of $Re^{-\frac{1}{2}}Nu$ values for various *Pr* estimates with $\gamma = F_c = \xi = Da = \phi = Ri = Ha = Nr = Ec = Q^* = 0$, $\varepsilon = 1$, and $\alpha = 90^0$.The acquired findings are compared with the published results of Shaiq et al. [56], Wang [57], and Reddy and Sidawi [58]. The results reported in the current study agree well with those obtained in previous investigations, thus we are certain that our findings are reliable.

## 5. Conclusions

The current contribution examines the nanofluid (SWCNTs/MWCNTs - water) flow over a stretching surface embedded in porous medium under the influence of inclined magnetic field, thermal radiation, viscous dissipation, and heat source factor. Dimensionless regulatory expressions are tackled using a local non-similarity approach in conjunction with the computational tool bvp4c. Physical quantity fluctuations are addressed and visualized using graphical and tabular approaches under various parametric circumstances. There is excellent

**Table 3**

Numerical outcomes of $Re^{\frac{1}{2}}C_f$ for SWCNTs-water and MWCNTs-water against the variation in several emerging parameters.

| $\phi$ | $\varepsilon$ | $\gamma$ | $Da$ | $Ha$ | $\alpha$ | $Ri$ | $-Re^{\frac{1}{2}}C_f$ SWCNTs-Water | $-Re^{\frac{1}{2}}C_f$ MWCNTs-Water |
|---|---|---|---|---|---|---|---|---|
| 0.00 | 0.9 | 0.7 | 0.02 | 0.5 | $60^0$ | 0.5 | 1.51328 | 1.51328 |
| 0.01 | | | | | | | 1.54492 | 1.53773 |
| 0.02 | | | | | | | 1.57727 | 1.56279 |
| 0.02 | 0.7 | 0.7 | 0.02 | 0.5 | $60^0$ | 0.5 | 1.42452 | 1.41141 |
| | 0.8 | | | | | | 1.50175 | 1.48795 |
| | 0.9 | | | | | | 1.57727 | 1.56279 |
| 0.02 | 0.9 | 0.5 | 0.02 | 0.5 | $60^0$ | 0.5 | 1.56719 | 1.55262 |
| | | 0.6 | | | | | 1.57224 | 1.55771 |
| | | 0.7 | | | | | 1.57727 | 1.56279 |
| 0.02 | 0.9 | 0.7 | 0.01 | 0.5 | $60^0$ | 0.5 | 2.15806 | 2.13762 |
| | | | 0.02 | | | | 1.57727 | 1.56279 |
| | | | 0.03 | | | | 1.32912 | 1.31727 |
| 0.02 | 0.9 | 0.7 | 0.02 | 0.5 | $60^0$ | 0.5 | 1.57727 | 1.56279 |
| | | | | 1.0 | | | 1.59910 | 1.58482 |
| | | | | 1.5 | | | 1.62065 | 1.60655 |
| 0.02 | 0.9 | 0.7 | 0.02 | 0.5 | $30^0$ | 0.5 | 1.56795 | 1.55339 |
| | | | | | $45^0$ | | 1.57323 | 1.55872 |
| | | | | | $60^0$ | | 1.57727 | 1.56279 |
| 0.02 | 0.9 | 0.7 | 0.02 | 0.5 | $60^0$ | 0.5 | 1.57727 | 1.56279 |
| | | | | | | 1.0 | 1.56153 | 1.54700 |
| | | | | | | 1.5 | 1.54618 | 1.53160 |

**Table 4**

Numerical outcomes of $Re^{-\frac{1}{2}}Nu$ for SWCNTs-water and MWCNTs-water against the variation in several emerging parameters.

| $\phi$ | $\varepsilon$ | $\gamma$ | $Ri$ | $Nr$ | $Ec$ | $Q^*$ | $Re^{-\frac{1}{2}}Nu$ SWCNTs-Water | $Re^{-\frac{1}{2}}Nu$ MWCNTs-Water |
|---|---|---|---|---|---|---|---|---|
| 0.00 | 0.9 | 0.7 | 0.5 | 0.5 | 0.01 | 0.1 | 1.45348 | 1.45348 |
| 0.01 | | | | | | | 1.40909 | 1.43881 |
| 0.02 | | | | | | | 1.36481 | 1.42292 |
| 0.02 | 0.7 | 0.7 | 0.5 | 0.5 | 0.01 | 0.1 | 2.00973 | 2.06622 |
| | 0.8 | | | | | | 1.69121 | 1.74895 |
| | 0.9 | | | | | | 1.36481 | 1.42292 |
| 0.02 | 0.9 | 0.7 | 0.5 | 0.5 | 0.01 | 0.1 | 1.36481 | 1.42292 |
| | | 0.8 | | | | | 1.32341 | 1.38084 |
| | | 0.9 | | | | | 1.28230 | 1.33911 |
| 0.02 | 0.9 | 0.7 | 0.5 | 0.5 | 0.01 | 0.1 | 1.36481 | 1.42292 |
| | | | 1.0 | | | | 1.51488 | 1.57088 |
| | | | 1.5 | | | | 1.64086 | 1.69564 |
| 0.02 | 0.9 | 0.7 | 0.5 | 0.4 | 0.01 | 0.1 | 1.35290 | 1.41134 |
| | | | | 0.5 | | | 1.36481 | 1.42292 |
| | | | | 0.6 | | | 1.37696 | 1.43458 |
| 0.02 | 0.9 | 0.7 | 0.5 | 0.5 | 0.01 | 0.1 | 1.36481 | 1.42292 |
| | | | | | 0.02 | | −0.05004 | −0.00121 |
| | | | | | 0.03 | | −1.46234 | −1.42267 |
| 0.02 | 0.9 | 0.7 | 0.5 | 0.5 | 0.01 | 0.00 | 2.62239 | 2.67541 |
| | | | | | | 0.05 | 2.05450 | 2.10883 |
| | | | | | | 0.10 | 1.36481 | 1.42292 |

**Table 5**

Comparison (as a limiting case) of outcomes for $-f''(0)$ against various values of $Ha$ with Andersson et al. [55] and Shaiq et al. [56] when $\varepsilon = 1$, $\alpha = 90^0$ and $\gamma = F_c = \xi = Da = \phi = Ri = Pr = Nr = Ec = Q^* = 0$.

| $Ha$ | Andersson et al. [55] | Shaiq et al. [56] | Present results |
|---|---|---|---|
| 0.5 | 1.225 | 1.2247 | 1.22511 |
| 1.0 | 1.414 | 1.4142 | 1.41428 |
| 1.5 | 1.581 | 1.5811 | 1.58115 |
| 2.0 | 1.732 | 1.7321 | 1.73205 |

**Table 6**

Comparison (as a limiting case) of outcomes for $-\theta'(0)$ against various values of $Pr$ with Shaiq et al. [56], Wang [57] and Reddy and Sidawi [58] when $\varepsilon = 1$, $\alpha = 90^0$ and $\gamma = F_c = \xi = Da = \phi = Ri = Ha = Nr = Ec = Q^* = 0$.

| $Pr$ | Shaiq et al. [56] | Wang [57] | Reddy and Sidawi [58] | Present results |
|---|---|---|---|---|
| 2.0 | 0.9144 | 0.9144 | 0.9144 | 0.91034 |
| 7.0 | 1.8954 | 1.8954 | 1.8954 | 1.89457 |
| 20 | 3.3539 | 3.3539 | 3.3539 | 3.35327 |
| 70 | 6.4622 | 6.4622 | 6.4622 | 6.46168 |

consistency between the current results and previously published outcomes in the literature. Finally, the assessment's innovative observations are summed up as follows:

- It is noted that increasing the nanoparticles concentration enhances the thermal profile of nanofluid.
- The decline in the velocity field with respect of magnetic field is clearly noticed.
- The boosting valuation of thermal radiation, heat source parameter, Eckert number and angle of inclination of magnetic field, nanofluid temperature profile is enhanced.
- The temperature profile of the SWCNTs-water is higher than that of the MWCNTs-water.
- Increment in Richardson and Darcy numbers leads to diminution of temperature profile.
- Velocity profiles for both SWCNTs/MWCNT-water nanofluids fall as the angle of inclination of magnetic field increases.
- It is seen that the Nusselt number decreases as Eckert number, nanoparticle volume fraction and heat generation factors are increased.
- At stretching surface MWCNTs-water nanofluid shows higher estimations of $Re^{-\frac{1}{2}}Nu$ than SWCNTs-water nanofluid.
- A comparative investigation is carried out to validate the current analysis, which establishes the consistency of the current results.
- As future work, it is proposed that the considered flow problem accomplished with different nanoparticles, fluid models and base liquids for optimum selection of nanofluid for heat transfer applications. The researchers can also simulate the current problem by considering two-phase Buongiorno nanofluid model and compare the outcomes with the advantages and drawbacks of each model.

## Nomenclature

| | |
|---|---|
| $x, y$ | Coordinates $(m)$ |
| $u, v$ | Velocity components $(ms^{-1})$ |
| $T$ | Temperature $(K)$ |
| $T_h$ | Surface temperature $(K)$ |
| $T_\infty$ | Ambient temperature $(K)$ |
| $U_\infty$ | Free stream velocity $(ms^{-1})$ |
| $\rho$ | Fluid density $(kgm^{-3})$ |
| $\alpha$ | Thermal diffusivity $(m^2/s)$ |
| $\beta$ | Thermal expansion coefficient $(K^{-1})$ |
| $\sigma$ | Electrical conductivity $(kg^{-1}m^{-3}s^3A^2)$ |
| $c_p$ | Specific heat $(m^2s^{-2}K^{-1})$ |
| $Q_0$ | Heat generation/absorption coefficient |
| $\mu$ | Viscosity $(kgm^{-1}s^{-1})$ |
| $K$ | Permeability $(m^2)$ |
| $\varepsilon$ | Porosity |
| $k$ | Thermal conductivity $(Wm^{-1}/K)$ |
| $B_0$ | Magnetic parameter$(kgs^{-2}A^{-1})$ |
| $\psi$ | Stream function $(m^2s^{-1})$ |
| $F_c$ | Forchheimer coefficient |
| $\phi$ | Nanoparticles concentration |
| $\alpha$ | Inclined angle of magnetic field |
| $f$ | dimensionless stream function |

| | |
|---|---|
| $\theta$ | Dimensionless temperature |
| $\xi$ | Non-similarity variable |
| $\eta$ | Pseudo-similarity variable |
| $Re_l$ | Reynolds number |
| $C_f$ | Skin friction coefficient |
| $Nu$ | Local Nusselt number |
| $\gamma$ | Darcy porosity parameter |
| $Da$ | Darcy number |
| $Ha$ | Hartmann number |
| $Pr$ | Prandtl number |
| $Ri$ | Richardson number |
| $Nr$ | Radiation parameter |
| $Q^*$ | Heat source/sink parameter |
| $Ec$ | Eckert number |
| $nf$ | Nanofluid |
| $bf$ | Base fluid |
| $pm$ | Porous medium |
| $np$ | Nanoparticles |

## Data availability statement

The data that support the findings of this study are available from the corresponding author upon reasonable request.

## Declaration of Competing Interest

The authors declare that they have no known competing financial interests or personal relationships that could have appeared to influence the work reported in this paper.

## Data availability

Data will be made available on request.

*Acknowledgement*

This work of Mikhail Sheremet was supported by the Tomsk State University Development Programme (Priority-2030).

## References

[1] C. Kleinstreuer, Z. Xu, Mathematical modeling and computer simulations of nanofluid flow with applications to cooling and lubrication, Fluids 1 (2) (2016) 16.
[2] A. Etbaeitabari, M. Barakat, A.A. Imani, G. Domairry, P. Jalili, An analytical heat transfer assessment and modeling in a natural convection between two infinite vertical parallel flat plates, J. Mol. Liq. 188 (2013) 252–257.
[3] M. Sheikholeslami, P. Jalili, D.D. Ganji, Magnetic field effect on nanofluid flow between two circular cylinders using AGM, Alexandria Eng. J. 57 (2) (2018) 587–594.
[4] P.K. Nagarajan, Influence of stability and particle shape effects for an entropy generation based optimized selection of magnesia nanofluid for convective heat flow applications, Appl. Surf. Sci. 489 (2019) 560–575.
[5] A.H. Pordanjani, S. Aghakhani, M. Afrand, M. Sharifpur, J.P. Meyer, H. Xu, H. Muhammad Ali, N. Karimi, G. Cheraghian, Nanofluids: physical phenomena, applications in thermal systems and the environment effects-a critical review, J. Clean. Prod. 320 (2021), 128573.
[6] R.P. Gowda, R.N. Kumar, B.C. Prasannakumara, B. Nagaraja, B.J. Gireesha, Exploring magnetic dipole contribution on ferromagnetic nanofluid flow over a stretching sheet: an application of Stefan blowing, J. Mol. Liq. 335 (2021), 116215.
[7] Y.X. Li, M.I. Khan, R.P. Gowda, A. Ali, S. Farooq, Y.M. Chu, S.U. Khan, Dynamics of aluminum oxide and copper hybrid nanofluid in nonlinear mixed Marangoni convective flow with entropy generation: applications to renewable energy, Chin. J. Phys. 73 (2021) 275–287.
[8] A. Raees, U. Farooq, M. Hussain, W.A. Khan, F.B. Farooq, Non-similar mixed convection analysis for magnetic flow of second-grade nanofluid over a vertically stretching sheet, Commun. Theor. Phys. 73 (6) (2021), 065801.
[9] B. Jalili, N. Aghaee, P. Jalili, D.D. Ganji, Novel usage of the curved rectangular fin on the heat transfer of a double-pipe heat exchanger with a nanofluid, Case Stud. Therm. Eng. 102086 (2022).
[10] M.M. Bhatti, M.B. Arain, A. Zeeshan, R. Ellahi, M.H. Doranehgard, Swimming of Gyrotactic microorganism in MHD Williamson nanofluid flow between rotating circular plates embedded in porous medium: application of thermal energy storage, J. Energy Storage 45 (2022), 103511.
[11] A. Shahid, M.M. Bhatti, R. Ellahi, K.S. Mekheimer, Numerical experiment to examine activation energy and bi-convection Carreau nanofluid flow on an upper paraboloid porous surface: application in solar energy, Sustain. Energy Technol. Assess. 52 (2022), 102029.
[12] M.A. Alazwari, N.H. Abu-Hamdeh, M. Goodarzi, Entropy optimization of first-grade viscoelastic nanofluid flow over a stretching sheet by using classical Keller-box scheme, Mathematics 9 (2021) 2563.
[13] N.H. Abu-Hamdeh, R.A. Alsulami, M.J.H. Rawa, M.A. Alazwari, M. Goodarzi, M. R. Safaei, A significant solar energy note on Powell-Eyring nanofluid with thermal jump conditions: implementing Cattaneo-Christov heat flux model, Mathematics 9 (2021) 2669.
[14] H. Aouinet, M. Dhahri, M.R. Safaei, H. Sammouda, A.E. Anqi, Turbulent boundary layers and hydrodynamic flow analysis of nanofluids over a plate, J. Cent. South Univ. 28 (2021) 3340–3353.
[15] W. Jamshed, S. Devi, M. Goodarzi, M. Prakash, K.S. Nisar, M. Zakarya, A.-H. Abdel-Aty, Evaluating the unsteady Casson nanofluid over a stretching sheet with solar thermal radiation: an optimal case study, Case Stud. Therm. Eng. 26 (2021), 101160.
[16] H. Maleki, M.R. Safaei, H. Togun, M. Dahari, Heat transfer and fluid flow of pseudo-plastic nanofluid over a moving permeable plate with viscous dissipation and heat absorption/generation, J. Therm. Anal. Calorim. 135 (2019) 1643–1654.
[17] T. Sajid, W. Jamshed, F. Shahzad, M.R. Eid, H.M. Alshehri, M. Goodarzi, E. K. Akgül, K.S. Nisar, Micropolar fluid past a convectively heated surface embedded with nth order chemical reaction and heat source/sink, Phys. Scr. 96 (10) (2021), 104010.
[18] H. Waqas, U. Farooq, S.A. Khan, H.M. Alshehri, M. Goodarzi, Numerical analysis of dual variable of conductivity in bioconvection flow of Carreau–Yasuda nanofluid containing gyrotactic motile microorganisms over a porous medium, J. Therm. Anal. Calorim. 145 (2021) 2033–2044.
[19] M. Imran, U. Farooq, H. Waqas, A.E. Anqi, M.R. Safaei, Numerical performance of thermal conductivity in bioconvection flow of cross nanofluid containing swimming microorganisms over a cylinder with melting phenomenon, Case Stud. Therm. Eng. 26 (2022) 101181.
[20] H. Maleki, J. Alsarraf, A. Moghanizadeh, H. Hajabdollahi, M.R. Safaei, Heat transfer and nanofluid flow over a porous plate with radiation and slip boundary conditions, J. Cent. South Univ. 26 (2019) 1099–1115.
[21] B. Jalili, H. Ghafoori, P. Jalili, Investigation of carbon nano-tube (CNT) particles effect on the performance of a refrigeration cycle, Int. J. Mater. Sci. Innov 2 (2014) 8–17.
[22] T. Gul, R.S. Gul, W. Noman, A. Saeed, S. Mukhtar, W. Alghamdi, H. Alrabaiah, CNTs-nanofluid flow in a rotating system between the gap of a disk and cone, Phys. Scr. 95 (12) (2020), 125202.
[23] H. Berrehal, O.D. Makinde, Heat transfer analysis of CNTs-water nanofluid flow between nonparallel plates: approximate solutions, Heat Transf. 50 (5) (2021) 4978–4992.
[24] W.F. Xia, S. Ahmad, M.N. Khan, H. Ahmad, A. Rehman, J. Baili, T.N. Gia, Heat and mass transfer analysis of nonlinear mixed convective hybrid nanofluid flow with multiple slip boundary conditions, Case Stud. Therm. Eng. 32 (2022), 101893.
[25] M. Hussain, J. Cui, U. Farooq, M.E. Ahmed Rabie, T. Muhammad, Nonsimilar modeling and numerical simulations of electromagnetic radiative flow of nanofluid with entropy generation, Math. Probl. Eng. 2022 (2022).
[26] R. Hossain, A.K. Azad, M.J. Hasan, M.M. Rahman, Thermophysical properties of kerosene oil-based CNT nanofluid on unsteady mixed convection with MHD and radiative heat flux, Eng. Sci. Technol. Int. J. 35 (2022), 101095.
[27] R.A. Mahdi, H.A. Mohammed, K.M. Munisamy, N.H. Saeid, Review of convection heat transfer and fluid flow in porous media with nanofluid, Renew. Sust. Energ. Rev. 41 (2015) 715–734.
[28] A. Kasaeian, R. Daneshazarian, O. Mahian, L. Kolsi, A.J. Chamkha, S. Wongwises, I. Pop, Nanofluid flow and heat transfer in porous media: a review of the latest developments, Int. J. Heat Mass Transf. 107 (2017) 778–791.
[29] A. Albojamal, K. Vafai, Analysis of particle deposition of nanofluid flow through porous media, Int. J. Heat Mass Transf. 161 (2020), 120227.
[30] D.K. Mandal, N. Biswas, N.K. Manna, R.S.R. Gorla, A.J. Chamkha, Role of surface undulation during mixed bioconvective nanofluid flow in porous media in presence of oxytactic bacteria and magnetic fields, Int. J. Mech. Sci. 211 (2021), 106778.
[31] F. Shahzad, W. Jamshed, K.S. Nisar, N.A.A.M. Nasir, R. Safdar, A.H. Abdel-Aty, I. S. Yahia, Thermal analysis for Al2O3–sodium alginate magnetized Jeffrey's nanofluid flow past a stretching sheet embedded in a porous medium, Sci. Rep. 12 (1) (2022) 1–14.
[32] T. Anusha, U.S. Mahabaleshwar, Y. Sheikhnejad, An MHD of nanofluid flow over a porous stretching/shrinking plate with mass transpiration and Brinkman ratio, Transp. Porous Media 142 (1) (2022) 333–352.
[33] B. Jalili, S. Sadighi, P. Jalili, D.D. Ganji, Characteristics of ferrofluid flow over a stretching sheet with suction and injection, Case Stud. Therm. Eng. 14 (2019), 100470.
[34] A. Mishra, M. Kumar, Thermal performance of MHD nanofluid flow over a stretching sheet due to viscous dissipation, joule heating and thermal radiation, Int. J. Appl. Comput. Math. 6 (4) (2020) 1–17.
[35] B. Jalili, P. Jalili, S. Sadighi, D.D. Ganji, Effect of magnetic and boundary parameters on flow characteristics analysis of micropolar ferrofluid through the shrinking sheet with effective thermal conductivity, Chin. J. Phys. 71 (2021) 136–150.
[36] B. Kumbhakar, S. Nandi, Unsteady MHD radiative-dissipative flow of cu-Al2O3/H2O hybrid nanofluid past a stretching sheet with slip and convective conditions: A regression analysis, Math. Comput. Simul. 194 (2022) 563–587.

[37] B. Jalili, S. Sadighi, P. Jalili, D.D. Ganji, Numerical analysis of MHD nanofluid flow and heat transfer in a circular porous medium containing a Cassini oval under the influence of the Lorentz and buoyancy forces, Heat Transf. (2022), https://doi.org/10.1002/htj.22582.
[38] W. Cheng, M. Safeer, U. Farooq, S. Munir, J. Cui, C.S. Raju, Nonsimilar forced convection simulations of water-copper nanofluid flow through a porous medium in the presence of thermal radiations, heat generation and viscous dissipation, Waves Random Complex Media (2022) 1–16.
[39] K. Padmaja, B.R. Kumar, Buoyancy and ohmic heating effects on MHD nanofluid flow over a vertical plate embedded in a porous medium, J. Porous Media 25 (8) (2022).
[40] E.U. Haq, S.U. Khan, T. Abbas, K. Smida, Q.M.U. Hassan, B. Ahmad, M. Ijaz Khan, K. Guedri, P. Kumam, A.M. Galal, Numerical aspects of thermo migrated radiative nanofluid flow towards a moving wedge with combined magnetic force and porous medium, Sci. Rep. 12 (1) (2022) 1–13.
[41] W. Cao, I.L. Animasaun, S.J. Yook, V.A. Oladipupo, X. Ji, Simulation of the dynamics of colloidal mixture of water with various nanoparticles at different levels of partial slip: ternary-hybrid nanofluid, Int. Commun. Heat Mass Transf. 135 (2022), 106069.
[42] S. Saleem, I.L. Animasaun, S.J. Yook, Q.M. Al-Mdallal, N.A. Shah, M. Faisal, Insight into the motion of water conveying three kinds of nanoparticles shapes on a horizontal surface: significance of thermo-migration and Brownian motion, Surf. Interf. 30 (2022), 101854.
[43] W. Xiu, I.L. Animasaun, Q.M. Al-Mdallal, A.K. Alzahrani, T. Muhammad, Dynamics of ternary-hybrid nanofluids due to dual stretching on wedge surfaces when volume of nanoparticles is small and large: forced convection of water at different temperatures, Int. Commun. Heat Mass Transf. 137 (2022), 106241.
[44] M. Hussain, U. Farooq, M. Sheremet, Nonsimilar convective thermal transport analysis of EMHD stagnation Casson nanofluid flow subjected to particle shape factor and thermal radiations, Int. Commun. Heat Mass Transf. 137 (2022), 106230.
[45] H.C. Brinkman, The viscosity of concentrated suspensions and solutions, J. Chem. Phys. 20 (1952) 571.
[46] B.C. Pak, Y.I. Cho, Hydrodynamic and heat transfer study of dispersed fluids with submicron metallic oxide particles, Exp. Heat Transf. Int. J. 11 (2) (1998) 151–170.
[47] Y. Xuan, W. Roetzel, Conceptions for heat transfer correlation of nanofluids, Int. J. Heat Mass Transf. 43 (19) (2000) 3701–3707.
[48] J.C. Maxwell, A Treatise on Electricity and Magnetism vol. 1, Clarendon press, 1873.
[49] Q.Z. Xue, Model for thermal conductivity of carbon nanotube-based composites, Phys. B Condens. Matter 368 (1–4) (2005) 302–307.
[50] A. Chamkha, R.S.R. Gorla, K. Ghodeswar, Non-similar solution for natural convective boundary layer flow over a sphere embedded in a porous medium saturated with a nanofluid, Transp. Porous Media 86 (1) (2011) 13–22.
[51] P. Rana, N. Shukla, Entropy generation analysis for non-similar analytical study of nanofluid flow and heat transfer under the influence of aligned magnetic field, Alexandria Eng. J. 57 (4) (2018) 3299–3310.
[52] U. Farooq, M. Hussain, M.A. Ijaz, W.A. Khan, F.B. Farooq, Impact of non-similar modeling on Darcy-Forchheimer-Brinkman model for forced convection of Casson nano-fluid in non-Darcy porous media, Int. Commun. Heat Mass Transf. 125 (2021), 105312.
[53] U. Farooq, W. Khan, M.I. Khan, F.B. Farooq, D. Lu, M.Y. Malik, E. Roshdy El-Zahar, Implication of forced convective flow of nanofluid towards an exponentially stretched surface: non-similar transformations, in: Proceedings of the Institution of Mechanical Engineers, Part E: Journal of Process Mechanical Engineering, 2022, 09544089221076694.
[54] E.M. Sparrow, H.S. Yu, Local Non-similarity Thermal Boundary-Layer Solutions, 1971.
[55] H.I. Andersson, K.H. Bech, B.S. Dandapat, Magnetohydrodynamic flow of a power-law fluid over a stretching sheet, Int. J. Non-Linear Mech. 27 (6) (1992) 929–936.
[56] S. Shaiq, E.N. Maraj, Z. Iqbal, Remarkable role of C3H8O2 on transportation of MoS2– SiO2 hybrid nanoparticles influenced by thermal deposition and internal heat generation, J. Phys. Chem. Solids 126 (2019) 294–303.
[57] C.Y. Wang, Free convection on a vertical stretching surface, ZAMM - J. Appl. Math. Mech. 69 (11) (1989) 418–420.
[58] R.S. Reddy Gorla, I. Sidawi, Free convection on a vertical stretching surface with suction and blowing, Appl. Sci. Res. 52 (3) (1994) 247–257.